Journal of Engineering Physics and Thermophysics, Vol. 79, No. 4, 2006

HYDROMAGNETIC CONVECTION FLOW THROUGH A POROUS MEDIUM IN AXIALLY VARYING PIPE

D. V. Krishna, D. R. V. Prasada Rao, and A. S. Ramachandra Murthy

UDC 536.25:537.84

The hydromagnetic mixed convection flow through a porous medium in a pipe of varying radius in a uniform axial magnetic field is analyzed. The pipe wall is maintained at a prescribed nonuniform temperature. The governing equations are solved analytically to obtain the velocity, temperature, and induced magnetic field. Their behaviors are evaluated for different variations in the governing parameters.

Introduction. During the last few decades, heat transfer in magnetic hydrodynamics (MHD) has been developed extensively under the combined stimuli of advances in geophysics and astrophysics. Most analytical works in MHD lead to either exact or approximate solution for unidirectional or two-dimensional channel flows in closed or series form. The channel may be partially bound and the disturbance is created due to thermal buoyancy. Several authors have worked in the above domains of MHD [1—5, 8, 9]. In the geothermal region, gases are electrically conducting, which is why they are affected by a magnetic field. The magnetothermal dynamics phenomenon in a porous medium results from the influence of a magnetic field on a conducting fluid flowing through the medium. Examination of the flow model reveals the combined influence of porosity and a magnetic field on the velocity and temperature profiles as well as on the local heat transfer. Reddy has discussed the effect of a magnetic field on the convective flow of an incompressible, viscous, electrically conducting fluid for different configurations of the pipe [10].

Convection flow through a channel of varying cross section creates a secondary flow which is of great importance to technological processes. In the hydromagnetic case, a flow through a channel with varying cross section has been considered by McMichael and Deutsch [6]. Here, the onset of flow separation is shown to be associated with adverse axial gradients of wall pressure created by radial magnetic forces. Those are produced by electric currents induced first of all by the zero-order streamlines crossing the uniform field, and large radial pressure gradients are obviously developed. Recently, Murthy has extended this problem to study the effects of a uniform axial magnetic field [7].

In this paper, we analyze the magnetohydrodynamic mixed convection flow through a porous medium in a pipe of varying radius in a uniform axial magnetic field. The pipe wall is maintained at a prescribed nonuniform temperature. The velocity, temperature, and induced field have axial and radial components, while the current density is characterized by an azimuthal component only. The components of the induced magnetic field are ultimately determined by matching conditions for the internal and external fields on the boundary. The behaviors of the velocity, temperature, and induced magnetic field obtained analytically are discussed and the corresponding profiles are presented for different sets of the governing parameters. The shear stress and the Nusselt number values are obtained.

Formulation and Solution of the Problem. We consider a steady axisymmetric flow of an incompressible, viscous, electrically conducting fluid through a porous medium in a vertical pipe of slowly varying cross section maintained at nonuniform temperature γ ($\delta x'/a$). The Boussinesq approximation is used; thus the density variations will be retained only in the buoyancy force. The viscous dissipation is neglected in comparison to the heat flow by convection. The cylindrical polar system $O(r, x)$ is chosen with the x-axis along the axis of the pipe. The boundary of the pipe is assumed to be

$$r' = af(\delta x'/a),$$

Department of Mathematics, S. K. University, Anantapur — 515003, (A.P.) India. Translated from Inzhenerno-Fizicheskii Zhurnal, Vol. 79, No. 4, pp. 96–104, July–August, 2006. Original article submitted May 27, 2004.

1062-0125/06/7904-0727

where a is the characteristic radius, f is a twice-differentiable function, and δ is a small parameter proportional to the boundary slope. The flow is maintained at a constant volume flow rate Q_{v} for which the characteristic velocity U is defined as

$$U = Q_{\mathrm{v}}/a^2 . \tag{1}$$

The applied magnetic field of induction $\mathbf{B}'$ is uniform and directed along the pipe axis. No electric field is applied and there is no induced electric field for the constraints given in [6]. The electrical conductivity of the pipe walls remains arbitrary and does not influence the fluid dynamics. We use the following nondimensional quantities:

$$\Delta T_{\mathrm{e}} = Qa^2/\lambda , \quad \theta = (T - T_{\mathrm{e}})/\Delta T_{\mathrm{e}} , \quad \boldsymbol{\zeta} = \boldsymbol{\zeta}' a/U ,$$

$$x = x'/a , \quad r = r'/a , \quad q = q'/U , \quad p = p'/(\rho U^2) , \quad \mathbf{B} = \mathbf{B}'/B_0 , \quad \mathbf{J} = \mathbf{J}'/(\sigma U B_0) .$$

Then the governing equations of the flow are

$$\mathrm{R}\,[\boldsymbol{\zeta} \times \mathbf{q} + \nabla\,(p + q^2/2)] = \nabla^2 \mathbf{q} - \sigma_1^2 \mathbf{q} + \mathrm{M}^2\,\mathbf{J} \times \mathbf{B} - \frac{G}{\mathrm{R}}\,\theta\,\frac{\mathbf{g}}{g} , \tag{2}$$

$$\nabla \cdot \mathbf{q} = 0 , \tag{3}$$

$$\mathrm{Pe}\,(\mathbf{q} \cdot \nabla)\,\theta = \theta_{rr} + (1/r)\,\theta_r + \theta_{xx} + 1 , \tag{4}$$

$$\nabla \cdot \mathbf{B} = 0 , \tag{5}$$

$$\nabla \times \mathbf{B} = \mathrm{R_m} \mathbf{J} , \tag{6}$$

$$\mathbf{J} = \mathbf{q} \times \mathbf{B} , \tag{7}$$

where

$$\mathrm{R} = Ua\rho/\mu , \quad \mathrm{R_m} = \sigma\mu_0 Ua , \quad \mathrm{M} = aB_0\,(\sigma/\mu)^{1/2} ,$$

$$\mathrm{Gr} = \beta g \Delta T_{\mathrm{e}} \rho^2 a^3/\mu^2 , \quad G = \mathrm{Gr}\,\frac{\Delta T_{\mathrm{e}}}{|\Delta T_{\mathrm{e}}|} , \quad \mathrm{Pe} = a\rho c_p U/\lambda , \quad \sigma_1^2 = a^2/k ,$$

and the subscripts r and x denote the respective partial derivatives. Under the constraints imposed, $\mathbf{J}$ has only the azimuthal component J_θ while $\mathbf{q}$ and $\mathbf{B}$ have axial and radial components:

$$\mathbf{q} = (u, v) , \quad \mathbf{B} = (f_1, f_2) .$$

The boundary conditions relevant to the problem are

$$v\,(r, x) = 0 , \quad \frac{\partial v}{\partial r} = 0 , \quad \frac{\partial T}{\partial r} = 0 \quad \text{at} \quad r = 0 ;$$

$$u\,(r, x) = 0 , \quad T - T_{\mathrm{e}} = \gamma\,(\delta x) \quad \text{at} \quad r = f .$$

Equations (2)—(7) constitute a system of six equations for six unknowns u, v, f_1, f_2, J_θ, *and* θ. *They can be reduced to the equations for the Stokes stream function* ψ *(*x, r) and the magnetic stream function $\phi(x, r)$ which are introduced in the following way:

$$u = -(1/r)\,\psi_r\,, \quad v = (1/r)\,\psi_x\,; \tag{8}$$

$$f_1 = -(1/r)\,\phi_r\,, \quad f_2 = (1/r)\,\phi_x\,. \tag{9}$$

Combining (7) and (8) to eliminate **J**, we find

$$E^2\phi = \mathrm{R_m}\,(1/r)\,(\psi_x\phi_r - \psi_x\phi_r)\,, \tag{10}$$

where the operator E^2 is defined as

$$E^2 = r\,\frac{\partial}{\partial r}\left((1/r)\,\frac{\partial}{\partial r}\right) + \frac{\partial^2}{\partial x^2}\,.$$

Substituting (7) into (2) and taking the curl of the latter to eliminate the pressure, we have

$$\mathrm{R}\,[(1/r)\,\psi_x\,(E^2\psi)_r - (1/r)\,\psi_r\,(E^2\psi)_x - (2/r^2)\,\psi_x E^2\psi] =$$

$$= E^4\psi + (\mathrm{M}^2/\mathrm{R_m})\,[(1/r)\,\phi_x\,(E^2\phi)_r - (1/r)\,\phi_r\,(E^2\phi)_x - (2/r^2)\,\phi_x E^2\phi]\ -$$

$$-\,(G/\mathrm{R})\,r\,\frac{\partial\theta}{\partial r} - \sigma_1^2 E^2\psi\,. \tag{11}$$

The energy equation is

$$\mathrm{Pe}\,(\theta_r\psi_x - \theta_x\psi_r) = \theta_{rr} + (1/r)\,\theta_r + \theta_{xx} + 1\,. \tag{12}$$

The current density can be found from Eq. (7), which reduces to

$$J_\theta = (1/r^2)\,(\psi_x\phi_r - \psi_r\phi_x)\,. \tag{13}$$

The coupled equations (11)—(13) are to be solved under the boundary conditions

$$\psi\,(r, x) = 0\,, \quad \frac{\partial}{\partial r}\left((1/r)\,\frac{\partial\psi}{\partial r}\right) = 0\,, \quad \frac{\partial\theta}{\partial r} = 0 \quad \text{at} \quad r = 0\,; \tag{14}$$

$$\psi\,(r, x) = -1/2\,, \quad \frac{\partial\psi}{\partial r} = 0\,, \quad \theta\,(r, x) = \gamma\,(\delta x) \quad \text{at} \quad r = f\,. \tag{15}$$

Hence the function ψ is that which assures a constant volumetric flow, in accord with (1), and the axial symmetry of the flow, according to conditions (14).

Electric currents within the fluid induce a magnetic field exterior to the pipe as well as within it. This external field $\hat{\mathbf{B}} = (\hat{f}_1, \hat{f}_2)$ is given by a potential $\hat{\mathbf{A}} = \hat{\phi}\mathbf{e}_\theta$, where $\mathbf{e}_\theta$ is the unit vector in the direction θ, so that

$$\hat{\mathbf{B}} = \nabla \times \hat{\mathbf{A}}$$

or

$$\hat{f}_1 = -(1/r)\,\hat{\phi}_r\,,\quad \hat{f}_2 = (1/r)\,\hat{\phi}_x\,.$$

Since $R_m = 0$ in the exterior region, Eq. (10) reduces to

$$E^2\hat{\phi} = 0\,. \tag{16}$$

Both the potential and the field itself must be continuous on the wall (at $r = f(x)$) [11]. Thus, we can write the following matching conditions:

$$\phi = \hat{\phi}\,,\quad \phi_r = \hat{\phi}_r \quad \text{at} \quad r = f(x)\,.$$

Following [6], we introduce the transformation

$$x = \delta x\,,\quad \eta = r/f(x)\,.$$

Solutions of the equations obtained are derived by perturbation analysis and are expressed through the modified Bessel functions.

Further we write the expressions for the stress tensor and the Nusselt number for the motion in the pipe. For example, the stress tensor is of the form

$$\sigma_{ij} = -p\delta_{ij} + 2\mu e_{ij}\,,$$

where

$$e_{xx} = \frac{\partial u}{\partial x}\,,\quad e_{rr} = \frac{\partial v}{\partial r}\,,\quad e_{rx} = \frac{1}{2}\left(\frac{\partial u}{\partial r} + \frac{\partial v}{\partial x}\right).$$

The shear stress on the pipe wall at $r = f(x)$ in dimensional form is given as

$$\tau = \sigma_{rx}(1 - f'^2) + (\sigma_{rr} - \sigma_{xx})f'(1 + f'^2)\,.$$

On the basis of the expressions for the shear stress and the Nusselt number, we can obtain the values of these characteristics for different sets of the governing parameters.

Results and Discussion. The velocity, temperature, shear stress, and Nusselt number for the pipe with varying radius are analytically evaluated and their behaviors with variations in the governing parameters G, R, σ_1, and β_1 are analyzed numerically. For computational purposes, the geometry of the pipe wall in the nondimensional form is assumed to be expressed as $r = f(\bar{x}) = 1 + \beta_1 \exp(-\bar{x}^2)$ and the prescribed wall temperature $\gamma(x)$ is chosen to be $\alpha \sin \bar{x}$. The cases of $\beta_1 > 0$ and $\beta_1 < 0$ correspond to the divergent and convergent pipe respectively. When the equilibrium temperature on the boundary is less than the actual temperature, G is positive; otherwise G is negative. The magnetic Reynolds number R_m is chosen to be $O(1)$ so that the induced magnetic field cannot be neglected in comparison to the applied field and thus influences the flow to some extent. In view of the magnetic flux condition, the current density vector **J** can be expressed in terms of the magnetic stream function ϕ and hence the governing equations are the coupled equations involving ψ, ϕ, and θ. Figures 1—4 give the profiles of u and v for different parametric values in both divergent and convergent pipes. It is of interest to note that the geometry of the boundary directly influences the occurrence of the convection cells. The porosity of the medium also affects the appearance of the reversal flows.

We see from Fig. 1a that, when a pipe is divergent, the axial flow is positive and hence no reversal flow occurs for $|G| \le 5 \cdot 10^3$. For $|G| \ge 10^4$, the reversal flow appears near the axis for $G > 0$ and near the boundary for $G < 0$. However, in a convergent pipe the reversal flow is absent in the entire domain for all G (Fig. 1c). When $G > 0$, the magnitude of u decreases near the axis with increase in G for a divergent pipe (but for $G \ge 10^4$, when u is negative, $|u|$ increases) and at intermediate values of η for a convergent pipe (Fig. 1a and c). A reversed dependence is observed for $G < 0$.

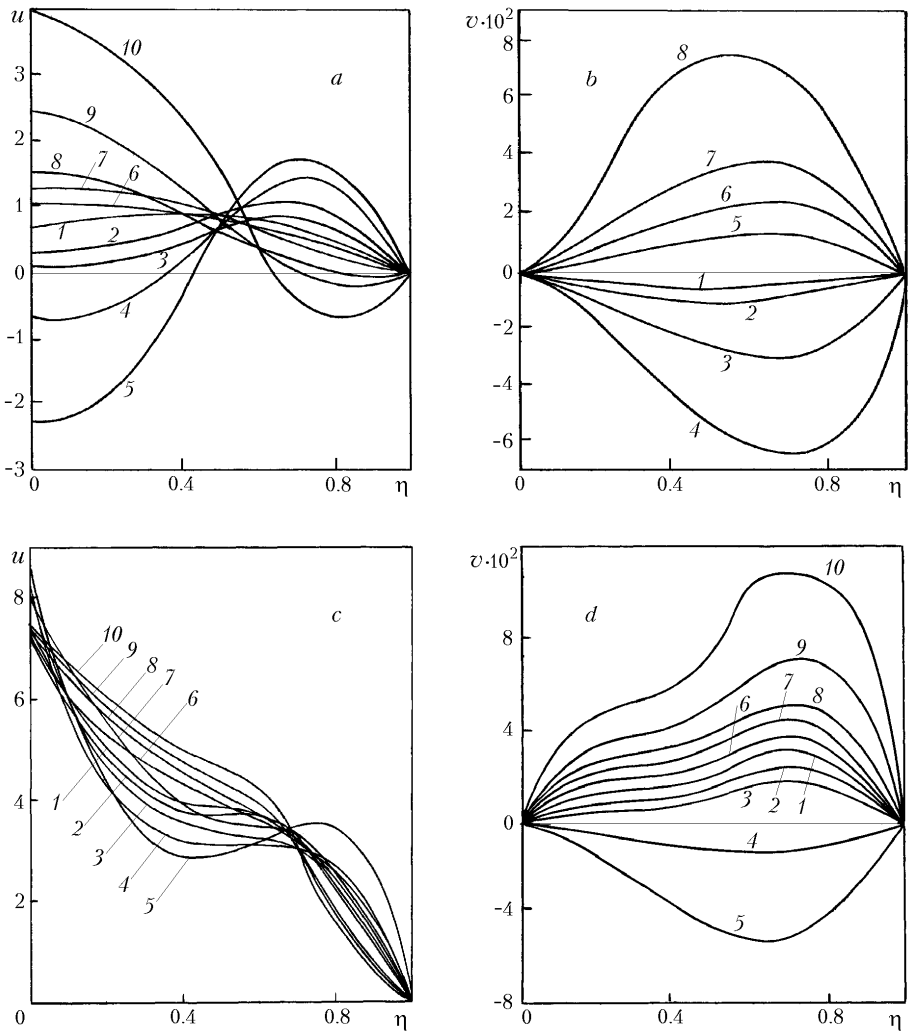

Fig. 1. Profiles of the axial (a and c) and radial (b and d) velocities for R = 50, $\alpha = 2$, $\sigma_1 = 2$ at $\beta_1 = 0.5$ (a and b) and $\beta_1 = -0.5$ (c and d) with different values of G: 1) $G = 10^3$; 2) $3\cdot10^3$; 3) $5\cdot10^3$; 4) 10^4; 5) $2\cdot10^4$; 6) -10^3; 7) $-3\cdot10^3$; 8) $-5\cdot10^3$; 9) -10^4; 10) $-2\cdot10^4$.

Figure 1b shows that the secondary velocity v in a divergent pipe is directed towards the axis for positive G (when $G \le 10^4$) and towards the boundary for negative G. We note that the magnitude of v increases with $|G|$ for all positive and negative G. In a convergent pipe, v is directed towards the boundary for all G except $G \ge 10^4$ (Fig. 1d). Here, $|v|$ decreases with increasing G when $G > 0$ and increases with $|G|$ when $G < 0$.

The values of u and v increase with R in the middle part of the channel, i.e., near the axis (Figs. 2a—d) and predominantly decrease in the remaining part adjacent to the boundary for all β_1 (Fig. 2a, c, and d). The value of u in the divergent pipe decreases with increasing σ_1 (i.e., with decreasing permeability) in both divergent and convergent pipes (Fig. 3a and c). It is of interest to see in Fig. 3a that for $\sigma_1 = 10$, the reversal flow appears near the axis even at the value of $G = 2\cdot10^3$, confirming that the appearance of convection cells depends highly on the porosity of the medium. We conclude that when the permeability of the medium is small, convection cells can appear even at smaller positive values of G in contrast to the case of larger permeability. The secondary flow exhibits different behavior for various geometries with variation in the porosity parameter. The value of $|v|$ in a divergent pipe decreases with increase in σ_1 (Fig. 3a), whereas in a convergent pipe it increases near the axis only (Fig. 3d). Figures 4a and b presents the profiles of u and v depending on the amplitude β_1. The surprising thing is that both $|u|$ and $|v|$ increase with $|\beta_1|$ in both divergent and convergent pipes.

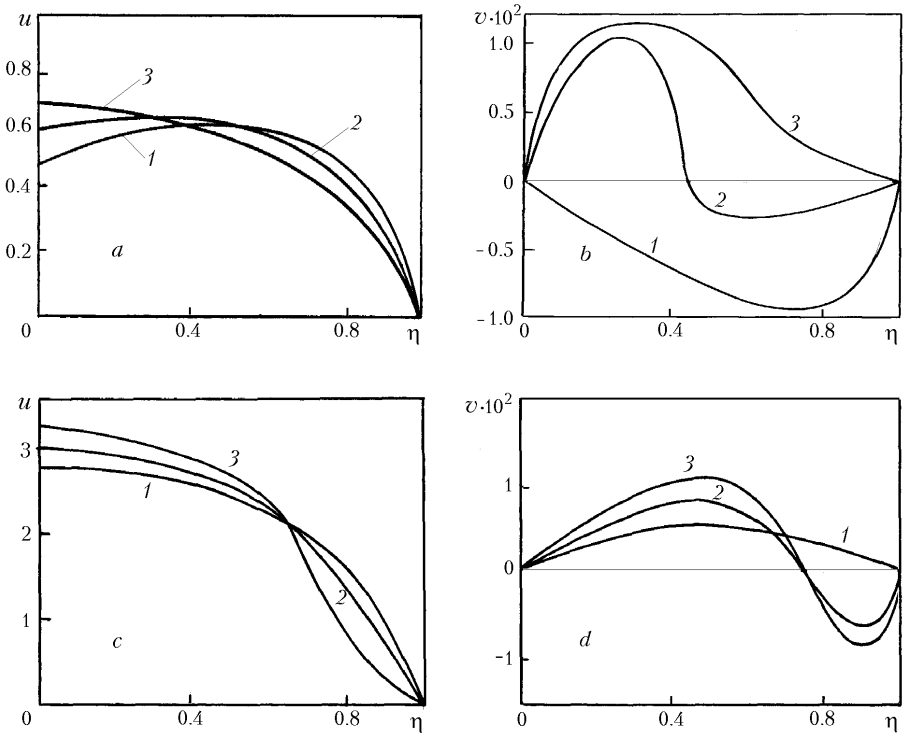

Fig. 2. Profiles of the axial (a and c) and radial (b and d) velocities for $G = 2 \cdot 10^3$, $\alpha = 2$ at $\beta_1 = 0.5$ (a and b) and $\beta_1 = -0.5$ (c and d) with different values of R: 1) R = 50; 2) 100; 3) 200.

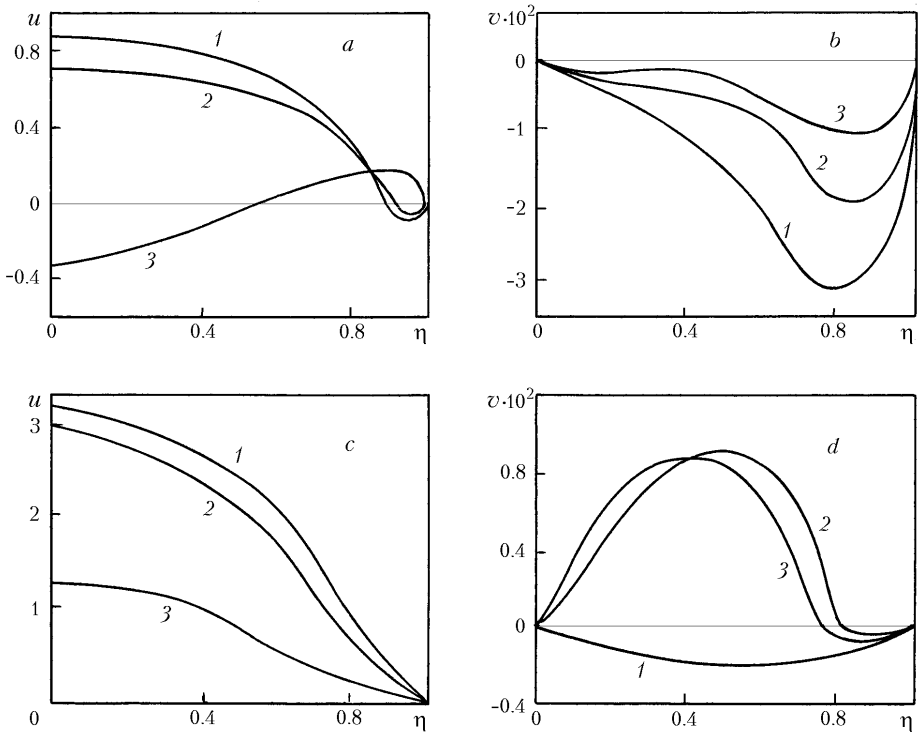

Fig. 3. Profiles of the axial (a and c) and radial (b and d) velocities for R = 50, $G = 2 \cdot 10^3$ at $\beta_1 = 0.5$ (a and b) and $\beta_1 = -0.5$ (c and d) with different values of σ_1: 1) $\sigma_1 = 1$; 2) 5; 3) 10.

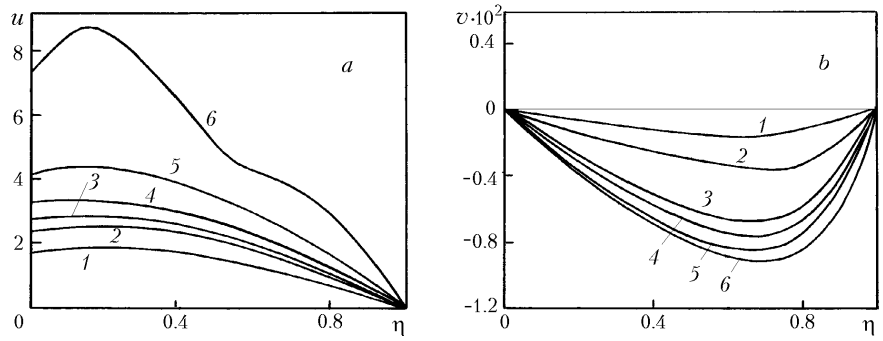

Fig. 4. Profiles of the axial (a) and radial (b) velocities for R = 50, $G = 2 \cdot 10^3$, and $\sigma_1 = 2$ with different values of β_1: 1) $\beta_1 = 0.5$; 2) 0.3; 3) 0.1; 4) –0.1; 5) –0.3; 6) –0.5.

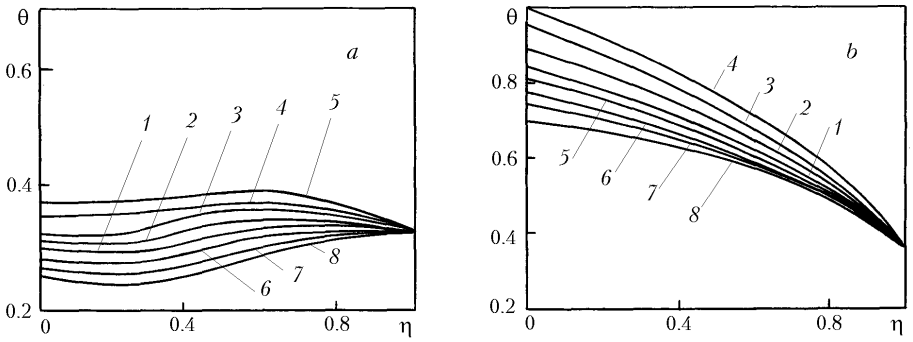

Fig. 5. Temperature profiles for R = 50, $\sigma_1 = 2$, and $\beta_1 = 0.5$ (a) and –0.5 (b) with different values of G: 1) $G = 10^3$; 2) $3 \cdot 10^3$; 3) $5 \cdot 10^3$; 4) 10^4; 5) $2 \cdot 10^4$; 6) -10^3; 7) $-3 \cdot 10^3$; 8) $-5 \cdot 10^3$.

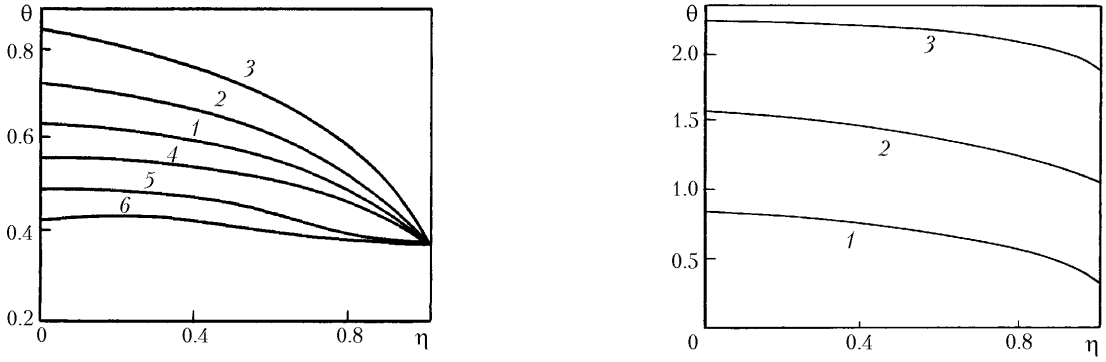

Fig. 6. Temperature profiles for R = 50, $\sigma_1 = 2$, and $G = 2 \cdot 10^3$ with different values of β_1: 1) $\beta_1 = 0.1$; 2) 0.3; 3) 0.5; 4) –0.1; 5) –0.3; 6) –0.5.

Fig. 7. Temperature profiles for R = 50, $\sigma_1 = 2$, $G = 2 \cdot 10^3$, and $\beta_1 = 0.5$ with different values of α: 1) $\alpha = 0.5$; 2) 1.5; 3) 2.5.

The temperature profiles for variations in G, β_1, α, and σ_1 are plotted in Figs. 5–8. It is seen from Fig. 5a and b that in both divergent and convergent pipes the temperature increases with G when $G > 0$ and decreases with increasing $|G|$ when G is negative (except for curve 5 in Fig. 5b). We also note that the greater the divergence and the less the convergence, the higher the temperature in the flow field over the whole cross section (Fig. 6). The temperature also increases with the amplitude of the wall-temperature distribution for $G > 0$ (Fig. 7) as well as with the porosity parameter in either of the pipe configurations (Fig. 8).

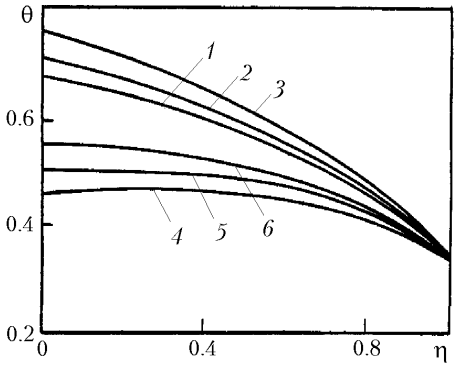

Fig. 8. Temperature profiles for R = 50 and $G = 2 \cdot 10^3$ with different values of σ_1 and β_1: 1) σ_1 = 1 and β_1 = 0.5; 2) 2 and 0.5; 3) 3 and 0.5; 4) 1 and –0.5; 5) 2 and –0.5; 6) 3 and –0.5.

As to shear stresses on the pipe, they are positive for $G > 0$ and in most cases are negative for $G < 0$. The value of stress increases with G for $G > 0$. An increase in R decreases τ for positive G and increases it for $G < 0$ (except for value at negative G with $|G|$ of the order of 10^4, where the reversal flow appears). Irrespective of the sign of the amplitude β_1, an increase in $|\beta_1|$ leads to a decrease in $|\tau|$. The stress increases in magnitude with the porosity parameter σ_1.

The average Nusselt number in general is negative except for certain cases of a convergent pipe for $G < 0$. These negative values of Nu imply that the temperature reaches its minimum in the vicinity of the wall before a rise to the prescribed value on the wall. We see that, all other parameters being equal, $|\mathrm{Nu}|$ increases with $|G|$ in both divergent and convergent pipes. Moreover , for $G > 0$ the value of $|\mathrm{Nu}|$ in a convergent pipe is much greater than in a divergent one, once again confirming that the heat transport in the first case is much more efficient. However, this situation gets reversed for smaller negative values of G when $|G| < 10^4$. An increase in $|\beta_1|$ in both pipes increases $|\mathrm{Nu}|$ for larger $|G|$. As the permeability of the medium reduces, the value of Nu becomes lower. We note that $|\mathrm{Nu}|$ decreases with increasing σ_1. For the most part, the wall-temperature parameter α does not affect the values of both stress and Nu.

CONCLUSIONS

1. The geometry of the boundary directly influences the occurrence of the convection cells. When $|G| > 10^4$ for a divergent pipe, the reversal flow occurs near the axis at positive G and near the boundary at negative G. In a convergent pipe, the reversal flow is absent.

2. The magnitude of the secondary velocity v decreases with $|G|$. The porosity parameter affects the appearance of the reversal flow. When the permeability of the medium is small, convection cells can appear even at smaller values of G in contrast to the case of large permeability of the medium.

3. The velocity rises with increase in both convergence and divergence.

4. The temperature increases with G when $G > 0$ and decreases with increasing $|G|$ when G is negative. The greater the divergence and the less the convergence, the higher the temperature in the flow field over the whole section.

5. The rate of heat transfer $|\mathrm{Nu}|$ increases with $|G|$ for both configurations.

6. For $G > 0$, the heat transport in a convergent pipe is much more efficient compared to a divergent one.

NOTATION

a, characteristic radius of the tube; **B**, magnetic induction; c_p, specific heat at constant pressure; f, nondimensional radius of the pipe; f_1 and f_2, components of magnetic induction; Gr, Grashof number; G, parameter connected with Gr; g, acceleration due to gravity; **J**, current density; k, permeability coefficient; M, Hartmann number; Nu,

Nusselt number; p, pressure; Pe, Peclet number; Q, external heat source; Q_v, flow rate; $\mathbf{q}$, velocity; R, Reynolds number; R_m, magnetic Reynolds number; r, radius of the pipe; T, temperature; U, characteristic velocity; u and v, nondimensional axial and radial components of velocity; x and r, axial and radial coordinates; α, wall temperature parameter; β, coefficient of volume expansion; β_1, pipe-radius parameter; γ, nondimensional boundary temperature; δ, small parameter; ξ, vorticity; θ, nondimensional temperature; λ, thermal conductivity; μ, viscosity; μ_0, magnetic permeability; ρ, density of the fluid; $\boldsymbol{\sigma}$, stress tensor; σ, electrical conductivity; σ_1, porosity parameter; τ, shear stress; ϕ, magnetic stream function; ψ, Stokes stream function. Subscripts and superscripts: e, equilibrium; 0, characteristic value; $'$, dimensional quantity; ^, external field.

REFERENCES

1. A. Bejan, On the boundary layer regime in a vertical enclosure filled with a porous medium, *Lett. Heat Mass Transfer*, **6**, 93—102 (1979).
2. S. A. Bories and M. A. Combarnous, Natural convection in a sloping porous layer, *J. Fluid. Mech.*, **57**, 68—79 (1973).
3. P. J. Burns, L. C. Chow, and C. L. Tien, Convection in a vertical slot filled with porous insulation, *Int. J. Heat Mass Transfer*, **20**, 919—926 (1976).
4. C. E. Hickox and D. K. Gartling, A numerical study of natural convection in a horizontal porous layer subjected to an end-to-end temperature difference, *ASME J. Heat Transfer*, **103**, 797—802 (1981).
5. P. H. Holst and K. Aziz, A theoretical and experimental study of natural convection in a confined porous medium, *Can. J. Chem. Eng.*, **50**, 232—241 (1972).
6. M. McMichael and S. Deutsch, Magnetohydrodynamic flow through an axially varying tube, *Phys. Fluids*, **27**, 110 (1984).
7. A. S. R. Murthy, MHD Convection Flow through a Non-Uniform Pipe, Ph.D. Thesis, S. K. University, Anantapur, A. P. India (1990).
8. Narasimha Rao and I. Pop, *Int. Comm. Heat Mass Transfer*, **21**, No. 4, 573—581 (1994).
9. V. Prasad and F. A. Kulacki, Natural convection in a vertical porous annulus, *Int. J. Heat Mass Transfer*, **27**, No. 2, 207—219 (1984).
10. A. R. Reddy, Computational Techniques in Hydromagnetic Convective Flows through a Porous Medium, Ph.D. Thesis, S. K. University, Anantapur, A. P. India (1997).
11. P. H. Roberts, *An Introduction to Magnetohydrodynamics*, Elsevier, New York (1967), p. 26.